Probing Site-Resolved Current in Strongly Interacting Superconducting Circuit Lattices

Botao Du, Ramya Suresh, Santiago López, Jeremy Cadiente, and Ruichao Ma*
Department of Physics and Astronomy, Purdue University, West Lafayette, Indiana 47907, USA

(Received 23 March 2024; accepted 8 July 2024; published 5 August 2024)

Transport measurements are fundamental for understanding condensed matter phenomena, from superconductivity to the fractional quantum Hall effect. Analogously, they can be powerful tools for probing synthetic quantum matter in quantum simulators. Here we demonstrate the measurement of *in situ* particle current in a superconducting circuit lattice and apply it to study transport in both coherent and bath-coupled lattices. Our method utilizes controlled tunneling in a double-well potential to map current to on-site density, revealing site-resolved current and current statistics. We prepare a strongly interacting Bose-Hubbard lattice at different lattice fillings, and observe the change in current statistics as the many-body states transition from superfluid to Mott insulator. Furthermore, we explore nonequilibrium current dynamics by coupling the lattice to engineered driven-dissipative baths that serve as tunable particle source and drain. We observe steady-state current in discrete conduction channels and interaction-assisted transport. These results establish a versatile platform to investigate microscopic quantum transport in superconducting circuits.

DOI: 10.1103/PhysRevLett.133.060601

Charge transport plays a crucial role in the exploration of quantum phases and phase transitions in condensed matter physics [1]. Electrical conductivity measurements probe the intrinsic properties of charge carriers, while current fluctuations from shot-noise measurements reveal the quantum dynamics and correlations of charge carriers in strongly interacting systems [2]. Meanwhile, synthetic quantum matter serve as emerging platforms for quantum simulation of condensed matter models, providing pristine many-body systems with exquisite control [3–5]. For instance, transport properties in ultracold atomic gases can be extracted from the time evolution of particle density either in response to an engineered non-uniform initial density [6,7] or to applied external forces [8]. In another example, the particle current through an atomic quantum point contact was measured by monitoring the particle number change in the attached finite-size reservoirs [9,10].

In superconducting (SC) quantum circuits, arrays of coupled SC qubits and resonators realize lattice models to study synthetic quantum matter comprised of interacting microwave photons [11–14]. Recent experiments have explored quantum states and dynamics in Bose-Hubbard lattices [15–20], many-body localization [21–23], entanglement generation and characterization [24–26], and flat-band physics [27,28]. Coherent transport of microwave photons has been probed via density measurements in a disordered lattice [23], and chiral current was measured in a triangular unit-cell with synthetic magnetic field [29]. SC circuits also provide an ideal playground to investigate nonequilibrium transport in driven-dissipative lattices [30–33], with recent experiments performing microwave transmission spectroscopy of driven-dissipative phases in 1D lattices [34–36]. Nevertheless, *in situ* control and measurement of transport dynamics remain less explored.

In this Letter, we demonstrate the direct measurement of site-resolved current and current statistics in a SC circuit lattice, and apply it to probe the change in current fluctuations across a superfluid to Mott insulator transition. Furthermore, we couple the lattice to engineered particle baths to induce and study non-equilibrium transport through discrete conduction channels of the interacting 1D lattice.

Measurement scheme—The scheme is based on Ref. [37] which we adapt to strongly interacting systems. We consider a Bose-Hubbard lattice [Fig. 1(a)] described by the Hamiltonian:

$$\mathcal{H}_{\mathrm{BH}}/\hbar = \sum_{\langle ij\rangle} J a_i^\dagger a_j + \frac{U}{2}\sum_i n_i(n_i-1) + \sum_i \epsilon_i n_i,$$

where $a_i^\dagger$ is the bosonic creation operator for a particle on site i, J is the nearest neighbor tunneling rate, U is the on-site interaction, $n_i = a_i^\dagger a_i$ is the on-site occupancy, ϵ_i is the local on-site energy, and $\hbar$ is the reduced Planck constant. The current operator $\hat{j}_{l\to r}$ for particles flowing from site l to site r is defined, from the continuity equation for local particle density, as [37]

$$\hat{j}_{l\to r} = iJ(a_l^\dagger a_r - a_r^\dagger a_l)$$

*Contact author: maruichao@purdue.edu

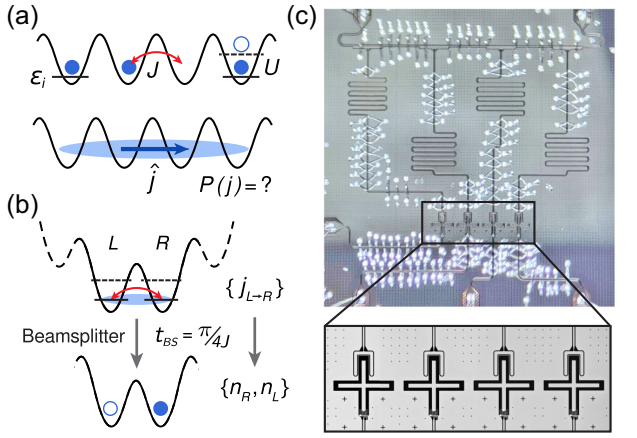

FIG. 1. Measurement scheme. (a) Illustration of a strongly interacting Bose-Hubbard lattice, and the particle current between two neighboring lattice sites. (b) Controlled tunneling in the double-well potential realizes a beam splitter operation that maps the nearest-neighbor current to on-site density. (c) Image of the superconducting circuit device with an enlarged view of the four-site transmon qubit lattice.

For noninteracting particles ($U \approx 0$), the current can be measured using an effective beam splitter operation (BS) implemented as controlled resonant tunneling between the two sites [37], illustrated in Fig. 1(b). After the evolution of an initial state in the isolated two-site system for a duration of $t_{\mathrm{BS}} = \pi/4J$, the initial current is mapped onto density imbalance according to $\hat{j}_{l\to r} \xrightarrow{\mathrm{BS}} J(n_r - n_l)$. As indicated from this mapping, the current operator $\hat{j}$ has discrete eigenvalues $j \in \{-nJ, -(n-1)J, \ldots, +nJ\}$, where $n = n_l + n_r$ is the total number of particles on the two sites. The current expectation value $\langle j \rangle$ and current statistics $P(j)$ are then extracted from a particle-number-resolved density measurement after the beam splitter operation. This current measurement method, applicable to noninteracting or weakly interacting particles, has been implemented in ultracold atoms to probe chiral currents albeit without spatial resolution [38] and recently in a quantum gas microscope to measure local current and current correlations [39].

Here, we extend this method to strongly interacting lattices in the hard-core boson limit ($U \gg J$). The on-site occupancy cannot exceed $n_i = 1$ under the hard-core condition, thereby limiting the current eigenvalues to $j \in \{-2J, -J, 0, +J, +2J\}$. We denote the on-site Fock states as $|0\rangle$ and $|1\rangle$. With the same resonant tunneling of duration t_{BS} between two sites, now in the presence of large U, the current eigenstates corresponding to $j = \{-J, 0, +J\}$ map uniquely to Fock states $\{|10\rangle, |00\rangle, |01\rangle\}$ after the beam splitter, i.e., $P(j = -J) \xrightarrow{\mathrm{BS}} P(|10\rangle)$, etc. The Fock state $|11\rangle$ does not evolve in density during the beam splitter operation in the hard-core limit, and can be written as an equal superposition of current eigenstates for $j = \pm 2J$. Therefore we obtain the probability of the remaining current components as $P(j = \pm 2J) \xrightarrow{\mathrm{BS}} \frac{1}{2}P(|11\rangle)$. From the current statistics, we calculate the current expectation value $\langle j \rangle = \sum_{j=-2}^{+2} jP(j)$. This protocol for measuring current is tailored for analog quantum simulation experiments in SC circuits, as it only requires density readout and does not rely on measuring phase-sensitive correlation functions. See Supplemental Material Sec. D for a detailed derivation of the current measurement [40].

SC circuit Bose-Hubbard lattice—In our SC circuit device, four transmon qubits [46] constitute the lattice sites of the 1D Bose-Hubbard lattice [Fig. 1(c)]. The capacitive coupling between neighboring transmons results in tunneling $J \approx 2\pi \times 6$ MHz, while the transmon anharmonicity provides the effective on-site interaction $U \approx -2\pi \times 246$ MHz. The on-site energies ϵ_i are given by the frequency of the transmon $n = 0 \to 1$ transition ω_{q} and dynamically tunable via individual on-chip flux lines. We typically operate the lattice near $\omega_{\mathrm{q}} \approx 2\pi \times 4.5$ GHz. Microwave photons in the lattice (transmon excitations) have a relaxation rate of $\Gamma_1 = 1/T_1 \approx 2\pi \times 5$ kHz and a dephasing rate of $\Gamma_\phi = 1/T_2^* \approx 2\pi \times 60$ kHz. Each transmon lattice site is capacitively coupled to an individual coplanar waveguide resonator used for dispersive readout of the on-site occupancy. We simultaneously measure all lattice sites by performing frequency-multiplexed readout via a common readout transmission line. See Supplemental Material [40] Secs. A–C for details on device parameters, measurement setup, and lattice control and characterization.

Current dynamics in a double well—To illustrate our protocol, we measure current in a resonant double well formed by two neighboring transmon lattice sites [Fig. 2(a)]. For any product state of the left and right sites with an initial population imbalance, we expect the density to start oscillating as a result of resonant tunneling and an oscillating current to develop between the two sites. Here we choose a product state with each site initialized in a superposition of $|1\rangle$ and $|0\rangle$. At the beginning of the experiment, the two sites start far detuned in frequency in their equilibrium ground states, which have approximately 6% thermal population in $|1\rangle$ due to the finite effective temperature of the device. We prepare superpositions with $P(|1\rangle)$ of 76% and 50% in the left and right sites, by applying two resonant microwave pulses that correspond to X rotations of 127° and 90° on the Bloch sphere of the transmon qubits. We then rapidly bring the two sites into resonance and evolve for a variable time before applying the current measurement protocol. The data are shown in Fig. 2(b), where we observe the coherent oscillation of the current $\langle j_{L\to R} \rangle$ with a period of π/J. Separately, we measure the on-site density in the double well and observe the population imbalance $\langle n_{\mathrm{R}} - n_{\mathrm{L}} \rangle$ oscillating 90° out of phase with the current, as expected

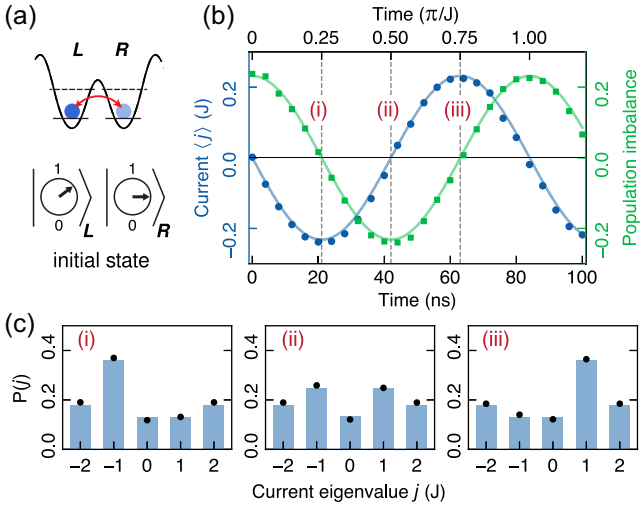

FIG. 2. Current dynamics in a resonant double well. (a) We start in a product state of two sites with unequal population. (b) Time evolution of current and population imbalance in the strongly interacting two-site system. (c) Current statistics at three different evolution times. Solid lines in (b) and bars in (c) are results from numerical simulation. Data shown in all figures are typically averaged over 40 000–100 000 experimental runs, with standard error of the mean smaller than the size of the data points. Other systematic uncertainties in the extracted density or current are below ±1%, see Supplemental Material [40] Sec. C.

from the relation between current and density under resonant tunneling discussed above. In this experiment, the density and current measurements share the same pulse sequence with the latter evolving for an extra duration of t_{BS} in the double well. The measured current statistics $P(j)$ at three different times are plotted in Fig. 2(c), revealing the origin of the observed current expectation value $\langle j\rangle$ and its quantum fluctuations. Because of the hard-core condition, the $j = \pm 2J$ components remain constant in time and contribute no net current. The oscillating nonzero current $\langle j\rangle$ comes from the $j = \pm J$ components as a result of single-particle tunneling in the double well. See Supplemental Material [40] Sec. D for calibration of the beam splitter operation.

Current statistics across the superfluid to Mott transition—We investigate current statistics in the hard-core Bose-Hubbard lattice at different average fillings $0 < \bar{n} \leq 1$. At unit filling, the state corresponds to the Mott insulator phase with suppressed density fluctuations [47]. At partial filling, the states are correlated superfluids where strong on-site interaction induces repulsive density correlations in the limit of 1D Tonks-Girardeau gases [18]. SC circuits provide a platform for new approaches to creating strongly correlated quantum states. Many-body states can be prepared spectroscopically via direct driving [26,48], or with disorder-assisted local adiabatic control [18]. Alternatively, engineered dissipation can serve as an effective chemical potential for microwave photons to stabilize many-body phases in SC circuits [49–52].

Here we prepare the Bose-Hubbard lattice at different fillings via adiabatic many-body Landau-Zener transitions using coherent external driving, similar to methods employed in recent Rydberg atom experiments [53]. As illustrated in Fig. 3(a), we apply a global microwave drive to all lattice sites via the readout transmission line. Starting with an empty lattice, we turn on the coherent drive to a Rabi amplitude $\Omega \approx 2\pi \times 4.2$ MHz in 300 ns. The initial drive frequency is detuned by $\Delta = 2\pi \times 30$ MHz $\approx 5J$ above the lattice frequency, away from all single-particle resonances which are within $\pm 2J$ of the lattice frequency. We then ramp the drive frequency at a constant rate of $-2\pi \times 80$ MHz/μs to populate the lattice through a sequence of avoided crossings between states of different total particle number N. The drive detuning at the end of the ramp is varied and determines the final lattice filling $\bar{n}$. Because of the relatively uniform drive amplitude and phase across the lattice sites, we prepare the highest energy states at different $\bar{n}$. Finally, we ramp down the drive

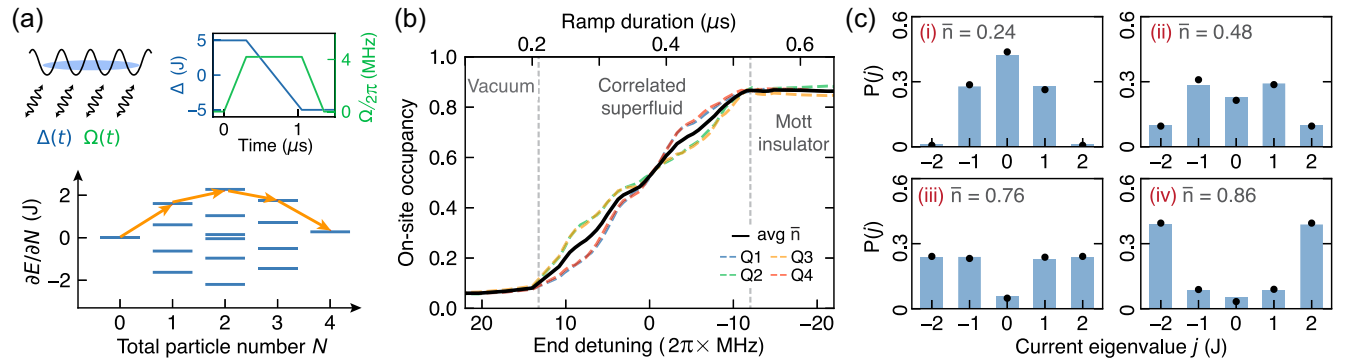

FIG. 3. Current statistics in a coherent Bose-Hubbard lattice. (a) Many-body states with different lattice fillings are prepared using a global coherent drive with time-varying amplitude and detuning. As the drive detuning varies, the lattice is adiabatically filled through a sequence of transitions in the many-body spectrum (orange arrows). (b) The measured on-site occupancy and average filling as a function of the drive end detuning. (c) Current statistics at four different lattice fillings, showing the change in the probability distribution. Bars show results from numerical simulation.

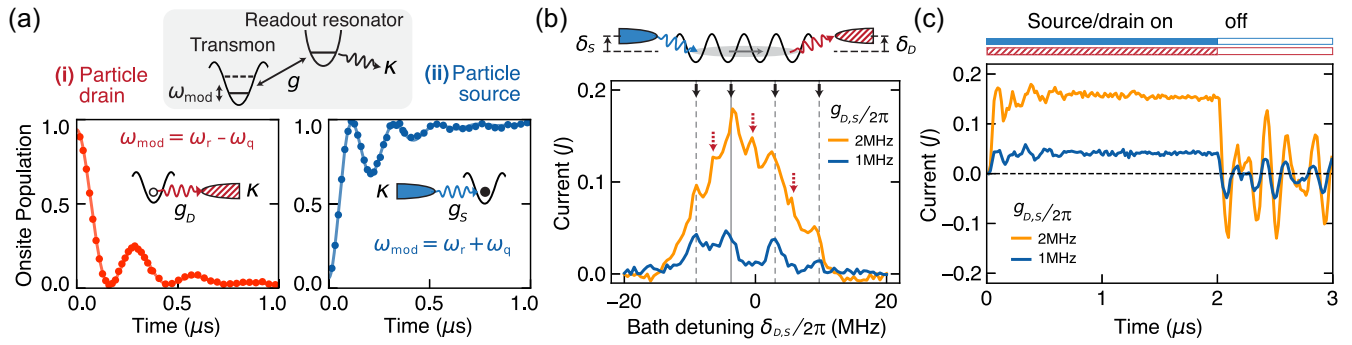

FIG. 4. Transport in a bath-coupled lattice. (a) We engineer local particle drain (i) and source (ii) by parametric coupling of the transmon and the lossy readout resonator. Plots show the dynamics of a single site coupled to the drain or source. Dots are experimental data; lines are numerical simulations. (b) Steady-state current through the lattice with end-coupled source and drain, measured as a function of bath detuning for two bath coupling rates. Black arrows on the current plot indicate frequencies of the single-particle eigenstates, and red dotted arrows indicate processes involving two-particle eigenstates. (c) Time dynamics of the current with the baths turned on at $t = 0$, then turned off at $t = 2$ μs after reaching steady state. The bath detuning in (c) is indicated by the solid line in (b).

amplitude to zero in 300 ns and then measure the resulting many-body state. Figure 3(b) shows the measured on-site occupancy and average lattice filling as a function of the drive end detuning. The final state transitions from the empty vacuum, to strongly-interacting superfluids at partial filling, to the Mott insulator at unit filling. To verify the adiabaticity of the preparation, we perform the coherent drive twice with a second reversed detuning ramp and measure the final lattice density. Due to finite thermal population, the lattice starts with $P(|0000\rangle) \approx 80\%$, and we extract a return probability of $P(|0000\rangle) \approx 60\%$ after the double ramp by comparing density data to numerical simulations. The preparation fidelity is consistent with theory and primarily limited by decoherence in the lattice. See Supplemental Material [40] Sec. E for the design and characterization of the drive parameters and additional analysis on adiabaticity.

The current statistics at different lattice fillings, measured between the two middle lattice sites, are shown in Fig. 3(c). For low filling $\bar{n} = 0.24$ $(N \approx 1)$, a single microwave photon is delocalized over the lattice, with strong fluctuations of the on-site occupancy. The current statistics is expected to follow a Skellam distribution [37] with a broad distribution peaked at $j = 0$. As $\bar{n}$ increases, both the density and current fluctuations are increasingly suppressed due to the strong interaction U. The observed $P(j)$ gradually becomes peaked at two eigenvalues $j = \pm 2J$, as a result of the Mott insulator at $\bar{n} = 1$ being the equal superposition of current eigenstates $j = \pm 2J$. The adiabatically prepared stationary states all have a vanishing mean current $\langle j \rangle$, as reflected in the symmetric distribution of the measured current statistics. The current statistics vary slightly at different locations in the finite lattice due to boundary effects but have the same qualitative features.

Nonequilibrium transport in bath coupled lattice—Finally, we explore particle transport in open lattices that are difficult to access in closed quantum systems or by local density measurements alone. We couple the two ends of the Bose-Hubbard lattice to particle source and drain, and measure current through the interacting 1D system. Such boundary-driven transport has been the subject of extensive theoretical investigations [54,55] and recently studied in a digital SC circuit experiment [52].

We utilize the transmon readout resonators as the source of dissipation to engineer local particle baths. The far-detuned resonators, with frequency $\omega_r \sim 2\pi \times (6.1\text{–}6.3)$ GHz and linewidth $\kappa \approx 2\pi \times 1.5$ MHz, are coupled to each transmon with $g \approx 2\pi \times 65$ MHz [Fig. 4(a)]. We generate resonant interactions between the transmon site and the resonator by parametric driving of the transmon flux line at frequency ω_{mod}. When $\omega_{\text{mod}} \approx \omega_r - \omega_q$, the flux driving modulates the on-site frequency and induces a coherent modulation-assisted tunneling between the transmon site and the resonator [56,57]. Since the resonator is lossy, this leads to an effective drain for microwave photons in the lattice. Alternatively when $\omega_{\text{mod}} \approx \omega_r + \omega_q$, the coherent parametric drive creates a pair of excitations, one to the transmon and one to the resonator [58]. One of the two excitations is lost via the resonator, leaving the other incoherently added to the transmon site—this leads to a particle source. We hence realize a hardware-efficient implementation of local baths anywhere in the lattice. The drain (D) and source (S) both have a narrow energy bandwidth of $\kappa \ll J$. The effective bath-lattice coupling rates $g_{\text{D,S}}$ and effective bath-lattice detunings $\delta_{\text{D,S}} = (|\omega_{\text{mod}} - \omega_r| - \omega_q)$ are dynamically tunable by controlling the amplitude and frequency of the parametric drive, respectively. Similar parametric driving processes are widely used in SC circuits for engineering tunable interactions [56–61].

In Fig. 4(a) (i), we plot the measured dynamics of an isolated site coupled resonantly to the drain with $\delta_D = 0$ and $g_D = 2\pi \times 1.75$ MHz. The site is initialized with one

photon and relaxes via its coupling with the drain to a steady-state population of $P(|1\rangle) = 0.02$, limited by the resonator thermal population. In (ii), an initially empty site is coupled to the source with $\delta_S = 0$ and $g_S = 2\pi \times 2.4$ MHz where the on-site population reaches a steady-state value of $P(|1\rangle) = 0.98$ in about 1 μs. In this device, we achieve maximum coupling rates of $g_D \sim 2\pi \times 12$ MHz limited by the flux tuning range of the transmon, and $g_S \sim 2\pi \times 4$ MHz limited by drive-induced heating.

To probe energy-dependent transport through the Bose-Hubbard lattice, we couple the source and drain to the ends of our 1D lattice with the same coupling rates and same detunings from the lattice [Fig. 4(b)]. After turning on the baths for 2 μs, we apply the current measurement protocol to the middle two lattice sites to measure the steady-state current $\langle j \rangle$ as a function of the bath detuning. At a relatively weak bath coupling of $g_{D,S} = 2\pi \times 1$ MHz, we observe four distinct current peaks when the narrow-band baths are tuned near the frequencies of the four single-particle eigenstates [i.e., $N = 1$ states in Fig. 3(a)]. We note that a finite current $\langle j \rangle$ requires coherent superposition between many-body eigenstates with the same particle number N. This follows from the observation that each energy eigenstate is stationary with vanishing $\langle j \rangle$, and the current operator commutes with particle number so eigenstates with different N contribute to the current independently. For weak bath coupling and low lattice filling, the measured steady-state current near each single-particle eigenfrequency originates from coherent admixtures between the resonantly driven single-particle eigenstate and other single-particle eigenstates that are off-resonantly excited by the finite-bandwidth bath. At a stronger bath coupling of $g_{D,S} = 2\pi \times 2$ MHz, we observe higher steady-state currents over a broader range of bath detuning. In addition to peaks at the single-particle eigenfrequencies, more peaks appear at the frequencies of $N = 2$ eigenstates which correspond to nonlinear transport processes where the baths add and remove two particles. Such processes are driven by the larger bath-lattice coupling and assisted by the effective interaction between many-body eigenstates that results from the on-site U. When eigenstates with more particles participate in the transport, the steady state current has contributions from superposition in different particle number manifolds. See Supplemental Material [40] Sec. G for detailed modeling of the bath-coupled steady-state current and current dynamics.

In Fig. 4(c), we measure the time evolution of the current at the specific bath detuning of $\delta_{D,S} = -2\pi \times 4$ MHz. After the source and drain are turned on at $t = 0$, we observe currents with initial oscillations that settle to the steady state value within 1 μs. At $t = 2$ μs, we turn off both baths and observe the subsequent current dynamics in the isolated lattice. The different eigenstates in the coherent superposition responsible for the steady-state current now evolve coherently at different eigenfrequencies. Therefore, the current undergoes coherent oscillations with a time-averaged value of zero. Alternatively, this can be viewed as the particles reflecting elastically at the edges of the lattice, moving back and forth with an oscillatory current. In bath-coupled lattices, the nonequilibrium steady state depends sensitively on the interplay between the coherent lattice interactions and parameters of the driven-dissipative baths [62–64]. Our future work will explore the detailed dependence of the steady-state current and current dynamics on the bath's spectral properties, lattice disorder, and decoherence, and many-body interactions.

Conclusion—In this Letter, we present the first measurement of site-resolved current *and* current statistics in an analog quantum simulator using SC circuits. We leveraged both coherent control and bath engineering to generate and probe nonequilibrium quantum transport in the Bose-Hubbard lattice, establishing a versatile setup for future exploration of open quantum systems and quantum thermodynamics [65,66]. Energy-dependent transport using tunable baths can be applied to probe critical behavior masked by transient finite-size effects in small closed systems [67]. Measuring current in the quantum critical regime, where the quasiparticle picture breaks down, will provide insights into the nature of collective excitations, how dissipation influences quantum critical dynamics, and how quantum entanglement evolves. For example, current statistics can reveal correlations and entanglement in many-body systems [68]. Furthermore, complex current correlation functions can be measured by simultaneous readout of multiple pairs of sites to investigate topological properties, e.g., in 2D lattices with chiral edge states [69,70].

Acknowledgments—We would like to thank Qi Zhou for stimulating discussions, and Srivatsan Chakram and Andrei Vrajitoarea for a careful reading of the manuscript. This work was supported by the National Science Foundation under Grant No. DMR-2145323, and the Air Force Office of Scientific Research under Grant No. FA9550-23-1-0491.

[1] S. Sachdev, *Quantum Phase Transitions* (Cambridge University Press, Cambridge, England, 2011).
[2] Y. M. Blanter and M. Büttiker, Phys. Rep. **336**, 1 (2000).
[3] I. M. Georgescu, S. Ashhab, and F. Nori, Rev. Mod. Phys. **86**, 153 (2014).
[4] E. Altman *et al.*, PRX Quantum **2**, 017003 (2021).
[5] A. J. Daley, I. Bloch, C. Kokail, S. Flannigan, N. Pearson, M. Troyer, and P. Zoller, Nature (London) **607**, 667 (2022).
[6] J.-Y. Choi, S. Hild, J. Zeiher, P. Schauß, A. Rubio-Abadal, T. Yefsah, V. Khemani, D. A. Huse, I. Bloch, and C. Gross, Science **352**, 1547 (2016).
[7] P. T. Brown, D. Mitra, E. Guardado-Sanchez, R. Nourafkan, A. Reymbaut, C.-D. Hébert, S. Bergeron, A.-M. S. Tremblay, J. Kokalj, D. A. Huse, P. Schauß, and W. S. Bakr, Science **363**, 379 (2019).
[8] R. Anderson, F. Wang, P. Xu, V. Venu, S. Trotzky, F. Chevy, and J. H. Thywissen, Phys. Rev. Lett. **122**, 153602 (2019).

[9] J.-P. Brantut, J. Meineke, D. Stadler, S. Krinner, and T. Esslinger, Science **337**, 1069 (2012).
[10] S. Häusler, S. Nakajima, M. Lebrat, D. Husmann, S. Krinner, T. Esslinger, and J.-P. Brantut, Phys. Rev. Lett. **119**, 030403 (2017).
[11] C. Noh and D. G. Angelakis, Rep. Prog. Phys. **80**, 016401 (2017).
[12] M. J. Hartmann, J. Opt. **18**, 104005 (2016).
[13] X. Gu, A. F. Kockum, A. Miranowicz, Y.-X. Liu, and F. Nori, Phys. Rep. **718–719**, 1 (2017).
[14] I. Carusotto, A. A. Houck, A. J. Kollár, P. Roushan, D. I. Schuster, and J. Simon, Nat. Phys. **16**, 268 (2020).
[15] S. Hacohen-Gourgy, V. V. Ramasesh, C. De Grandi, I. Siddiqi, and S. M. Girvin, Phys. Rev. Lett. **115**, 240501 (2015).
[16] M. C. Collodo, A. Potočnik, S. Gasparinetti, J.-C. Besse, M. Pechal, M. Sameti, M. J. Hartmann, A. Wallraff, and C. Eichler, Phys. Rev. Lett. **122**, 183601 (2019).
[17] R. Ma, B. Saxberg, C. Owens, N. Leung, Y. Lu, J. Simon, and D. I. Schuster, Nature (London) **566**, 51 (2019).
[18] B. Saxberg, A. Vrajitoarea, G. Roberts, M. G. Panetta, J. Simon, and D. I. Schuster, Nature (London) **612**, 435 (2022).
[19] A. Morvan *et al.*, Nature (London) **612**, 240 (2022).
[20] X. Zhang, E. Kim, D. K. Mark, S. Choi, and O. Painter, Science **379**, 278 (2023).
[21] P. Roushan *et al.*, Science **358**, 1175 (2017).
[22] Q. Guo, C. Cheng, H. Li, S. Xu, P. Zhang, Z. Wang, C. Song, W. Liu, W. Ren, H. Dong, R. Mondaini, and H. Wang, Phys. Rev. Lett. **127**, 240502 (2021).
[23] Q. Guo, C. Cheng, Z.-H. Sun, Z. Song, H. Li, Z. Wang, W. Ren, H. Dong, D. Zheng, Y.-R. Zhang, R. Mondaini, H. Fan, and H. Wang, Nat. Phys. **17**, 234 (2021).
[24] J. Braumüller, A. H. Karamlou, Y. Yanay, B. Kannan, D. Kim, M. Kjaergaard, A. Melville, B. M. Niedzielski, Y. Sung, A. Vepsäläinen, R. Winik, J. L. Yoder, T. P. Orlando, S. Gustavsson, C. Tahan, and W. D. Oliver, Nat. Phys. **18**, 172 (2022).
[25] P. Zhang *et al.*, Nat. Phys. **19**, 120 (2023).
[26] A. H. Karamlou, I. T. Rosen, S. E. Muschinske, C. N. Barrett, A. D. Paolo, L. Ding, P. M. Harrington, M. Hays, R. Das, D. K. Kim, B. M. Niedzielski, M. Schuldt, K. Serniak, M. E. Schwartz, J. L. Yoder, S. Gustavsson, Y. Yanay, J. A. Grover, and W. D. Oliver, Nature (London) **629**, 561 (2024).
[27] A. J. Kollár, M. Fitzpatrick, and A. A. Houck, Nature (London) **571**, 45 (2019).
[28] J. G. C. Martinez, C. S. Chiu, B. M. Smitham, and A. A. Houck, Sci. Adv. **9**, eadj7195 (2023).
[29] P. Roushan *et al.*, Nat. Phys. **13**, 146 (2017).
[30] M. Leib and M. J. Hartmann, New J. Phys. **12**, 093031 (2010).
[31] A. Biella, L. Mazza, I. Carusotto, D. Rossini, and R. Fazio, Phys. Rev. A **91**, 053815 (2015).
[32] T. Mertz, I. Vasić, M. J. Hartmann, and W. Hofstetter, Phys. Rev. A **94**, 013809 (2016).
[33] A. A. Bychek, P. S. Muraev, D. N. Maksimov, and A. R. Kolovsky, Phys. Rev. E **101**, 012208 (2020).
[34] M. Fitzpatrick, N. M. Sundaresan, A. C. Y. Li, J. Koch, and A. A. Houck, Phys. Rev. X **7**, 011016 (2017).
[35] G. P. Fedorov, S. V. Remizov, D. S. Shapiro, W. V. Pogosov, E. Egorova, I. Tsitsilin, M. Andronik, A. A. Dobronosova, I. A. Rodionov, O. V. Astafiev, and A. V. Ustinov, Phys. Rev. Lett. **126**, 180503 (2021).
[36] A. Vrajitoarea, R. Belyansky, R. Lundgren, S. Whitsitt, A. V. Gorshkov, and A. A. Houck, arXiv:2209.14972.
[37] S. Keßler and F. Marquardt, Phys. Rev. A **89**, 061601(R) (2014).
[38] M. Atala, M. Aidelsburger, M. Lohse, J. T. Barreiro, B. Paredes, and I. Bloch, Nat. Phys. **10**, 588 (2014).
[39] A. Impertro, S. Karch, J. F. Wienand, S. Huh, C. Schweizer, I. Bloch, and M. Aidelsburger, arXiv:2312.13268 [Phys. Rev. Lett. (to be published)].
[40] See Supplemental Material at http://link.aps.org/supplemental/10.1103/PhysRevLett.133.060601 for device characterization, measurement setup, numerical modeling, and additional analysis of the data, which includes Refs. [41–45].
[41] M. A. Rol, L. Ciorciaro, F. K. Malinowski, B. M. Tarasinski, R. E. Sagastizabal, C. C. Bultink, Y. Salathe, N. Haandbaek, J. Sedivy, and L. DiCarlo, Appl. Phys. Lett. **116**, 054001 (2020).
[42] B. R. Johnson, Controlling photons in superconducting electrical circuits, Ph.D. thesis, Yale University, Ann Arbor, United States, 2011.
[43] K. Geerlings, Z. Leghtas, I. M. Pop, S. Shankar, L. Frunzio, R. J. Schoelkopf, M. Mirrahimi, and M. H. Devoret, Phys. Rev. Lett. **110**, 120501 (2013).
[44] F. Pedregosa, G. Varoquaux, A. Gramfort, V. Michel, B. Thirion, O. Grisel, M. Blondel, P. Prettenhofer, R. Weiss, V. Dubourg, J. Vanderplas, A. Passos, D. Cournapeau, M. Brucher, M. Perrot, and E. Duchesnay, J. Mach. Learn. Res. **12**, 2825 (2011), http://jmlr.org/papers/v12/pedregosa11a.html.
[45] G. Roberts, A. Vrajitoarea, B. Saxberg, M. G. Panetta, J. Simon, and D. I. Schuster, Sci. Adv. **10**, ado1069 (2024).
[46] J. Koch, T. M. Yu, J. Gambetta, A. A. Houck, D. I. Schuster, J. Majer, A. Blais, M. H. Devoret, S. M. Girvin, and R. J. Schoelkopf, Phys. Rev. A **76**, 042319 (2007).
[47] W. S. Bakr, A. Peng, M. E. Tai, R. Ma, J. Simon, J. I. Gillen, S. Fölling, L. Pollet, and M. Greiner, Science **329**, 547 (2010).
[48] R. O. Umucalılar and I. Carusotto, Phys. Rev. A **96**, 053808 (2017).
[49] M. Hafezi, P. Adhikari, and J. M. Taylor, Phys. Rev. B Condens. Matter **92**, 174305 (2015).
[50] J. Lebreuilly and I. Carusotto, C.R. Phys. **19**, 433 (2018).
[51] R. Ma, C. Owens, A. Houck, D. I. Schuster, and J. Simon, Phys. Rev. A **95**, 043811 (2017).
[52] X. Mi *et al.*, Science **383**, 1332 (2024).
[53] S. de Léséleuc, V. Lienhard, P. Scholl, D. Barredo, S. Weber, N. Lang, H. P. Büchler, T. Lahaye, and A. Browaeys, Science **365**, 775 (2019).
[54] G. T. Landi, D. Poletti, and G. Schaller, Rev. Mod. Phys. **94**, 045006 (2022).
[55] B. Bertini, F. Heidrich-Meisner, C. Karrasch, T. Prosen, R. Steinigeweg, and M. Žnidarič, Rev. Mod. Phys. **93**, 025003 (2021).

[56] F. Beaudoin, M. P. da Silva, Z. Dutton, and A. Blais, Phys. Rev. A **86**, 022305 (2012).
[57] J. D. Strand, M. Ware, F. Beaudoin, T. A. Ohki, B. R. Johnson, A. Blais, and B. L. T. Plourde, Phys. Rev. B Condens. Matter **87**, 220505(R) (2013).
[58] Y. Lu, S. Chakram, N. Leung, N. Earnest, R. K. Naik, Z. Huang, P. Groszkowski, E. Kapit, J. Koch, and D. I. Schuster, Phys. Rev. Lett. **119**, 150502 (2017).
[59] C. Macklin, K. O'Brien, D. Hover, M. E. Schwartz, V. Bolkhovsky, X. Zhang, W. D. Oliver, and I. Siddiqi, Science **350**, 307 (2015).
[60] R. K. Naik, N. Leung, S. Chakram, P. Groszkowski, Y. Lu, N. Earnest, D. C. McKay, J. Koch, and D. I. Schuster, Nat. Commun. **8**, 1904 (2017).
[61] M. Reagor *et al.*, Sci. Adv. **4**, eaao3603 (2018).
[62] G. Kordas, D. Witthaut, P. Buonsante, A. Vezzani, R. Burioni, A. I. Karanikas, and S. Wimberger, Eur. Phys. J. Spec. Top. **224**, 2127 (2015).
[63] L. M. Sieberer, M. Buchhold, and S. Diehl, Rep. Prog. Phys. **79**, 096001 (2016).
[64] S. Dutta and N. R. Cooper, Phys. Rev. Res. **3**, L012016 (2021).
[65] F. Binder, L. A. Correa, C. Gogolin, J. Anders, and G. Adesso, *Thermodynamics in the Quantum Regime: Fundamental Aspects and New Directions* (Springer, New York, 2019).
[66] S. Deffner and S. Campbell, *Quantum Thermodynamics: An Introduction to the Thermodynamics of Quantum Information* (Morgan & Claypool Publishers, San Rafael, CA, 2019).
[67] Z. Lenarčič, O. Alberton, A. Rosch, and E. Altman, Phys. Rev. Lett. **125**, 116601 (2020).
[68] I. Klich and L. Levitov, Phys. Rev. Lett. **102**, 100502 (2009).
[69] B. M. Anderson, R. Ma, C. Owens, D. I. Schuster, and J. Simon, Phys. Rev. X **6**, 041043 (2016).
[70] J. C. Owens, M. G. Panetta, B. Saxberg, G. Roberts, S. Chakram, R. Ma, A. Vrajitoarea, J. Simon, and D. I. Schuster, Nat. Phys. **18**, 1048 (2022).